

Received September 2, 2019, accepted September 10, 2019, date of publication September 18, 2019, date of current version October 2, 2019.

Digital Object Identifier 10.1109/ACCESS.2019.2942038

Magnet Shape Design and Verification for SPMSM of EPS System Using Cycloid Curve

HYEON-JIN PARK¹, MYUNG-SEOP LIM¹, AND CHUNG-SEONG LEE²

¹Department of Automotive Engineering, Hanyang University, Seoul 04763, South Korea

²Advanced Research and Development Center, Mando Corporation, Seongnam 13486, South Korea

Corresponding author: Chung-Seong Lee (chungseong.lee@halla.com)

ABSTRACT A low cogging torque and torque ripple are the most important qualities for electric power steering (EPS) motors. Therefore, various design methods are employed to obtain EPS motors with these qualities. In this study, a novel design method for the pole shape was developed by adopting a cycloid curve to realize the desired qualities of EPS motors without reducing the torque. An evaluation index (δq) was used to design the pole shape of the magnet and to compare the pole shape between the proposed method and the conventional method. The proposed and conventional methods were applied to existing machine designs, and their performances were compared using a finite-element analysis (FEA). The results of the FEA and prototype tests indicated an improved motor performance for the proposed method.

INDEX TERMS Electric power steering (EPS), surface permanent magnet synchronous machine (SPMSM), cycloid curve, cogging torque, torque ripple.

NOMENCLATURE

R_{si}	Stator inner radius
R_{mo}	Rotor outer radius
τ_p	Pole pitch angle
τ_a	Pole arc angle
g	Air gap length
t_m	Magnet thickness
R_{ri}	Rotor core outer radius
B_r	Remanent flux density
R_{fc}	Fixed circle radius
R_{rc}	Rolling circle radius
n	Integer divided R_{fc} by R_{rc}
O_{fc}	Center point for R_{fc}
O_{rc}	Center point for R_{rc}
P_c	A point on cycloid curve
ε_c	Eccentricity from O_{rc}
N_p	Pole numbers
P_{cet}	A point on the cycloid CET
P_{pet}	A point on the cycloid PET
P_{min}	Point which the length ε_c is rotated by O_{rcmin}
δq	Length from P_{min} to R_{mo}
R_{ec}	Eccentric circle radius
ε_e	Eccentricity of Eccentric circle

The associate editor coordinating the review of this manuscript and approving it for publication was Giambattista Gruosso.

I. INTRODUCTION

Electric machines are widely used for a variety of applications. Owing to its high efficiency and torque density, the permanent magnet (PM) motor is commonly applied to electric power steering (EPS) systems [1], [2]. For many applications, the cogging torque and torque ripple for an electric motor are significant [3]–[5]. This is also true for the surface PM (SPM) employed in vehicle EPS systems [6]. The motor requires a low cogging torque and torque ripple for comfortable vehicle steering [7]. An electromagnetic design for reductions of the cogging torque and torque ripple is applied using various design methods. The first method is step skewing in a rotor or stator [5]. This design method is commonly adopted in industry. However, as the amount of step skewing increases, the torque reduction increases owing to axial flux leakage, and the assembly cost increases [8], [9]. The second method involves applying a pole-shape design of a magnet in an SPM and a rotor core in an internal PM. This method reduces the back electromotive force (EMF) by implementing an air-gap flux wave as a sinusoidal wave [10]–[13]. Eccentric curves are widely used in the pole-shape design method [11]–[13]. In this paper, a cycloid curve of a magnet in an SPM is proposed for such a method.

The pole shape of the proposed magnet design method uses selected cycloids. No studies have been performed in which cycloids were applied to the pole-shape design in an

electric motor, although cycloids have been applied to magnetic gears, having the function of increasing the torque using an electromagnetic force instead of a mechanical contact, as in the case of a conventional speed reducer [14]–[16]. However, the cycloid curve has not been directly applied to the pole shape of a magnet. In general, the cycloid curve is applied to the geometry of the teeth of a cycloid reducer in a mechanical reducer [17].

In this study, to compare and evaluate the cycloid and conventional curves, a design method using an evaluation index (δq) was developed. By applying δq , the motor performance, including the cogging torque and torque ripple, was compared for cycloid and conventional curves.

Prototypes were manufactured to verify the results of a finite-element analysis (FEA) and perform a prototype test. The results of the FEA and prototype tests indicated that the motor performance of the proposed method was improved.

II. CYCLOID CURVE

A. DEFINITION AND TYPE

In general, a cycloid is a curve traced by a point on a circle rolling along a fixed circle without slippage. Thus, a cycloid curve can be classified into six types, as shown in Table 1, according to the position of the tracing point on the rolling wheel [17].

B. SELECTION AND CURVE EQUATION

Among the cycloid-curve types, the curves applicable to the magnet shape of the surface permanent magnet synchronous machine (SPMSM) are an epitrochoid, a curtate epitrochoid (CET), and prolate epitrochoid (PET), as shown in Table 1. In the case of an epitrochoid, the cycloid is determined by the radius of the circle on which the rolling wheel rolls; thus, an epitrochoid cannot express various shapes of a curve compared with a CET or PET. Therefore, when an epicycloid curve is applied to a magnet shape, the analysis of the motor performance is limited.

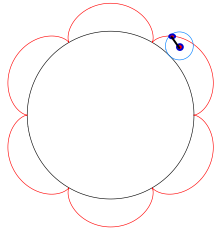
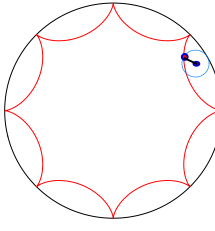
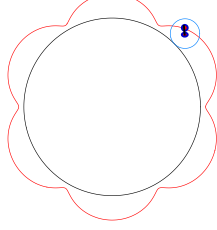
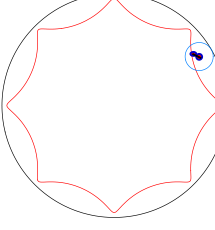
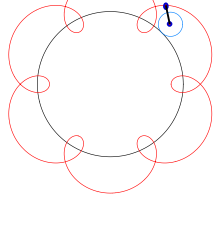
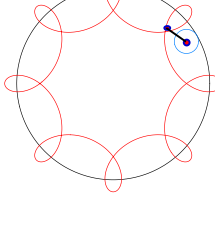
Because this limit is the same for a speed reducer applying the aforementioned cycloid tooth types, to create a design that satisfies the required performance, the eccentricity of the point is adjusted to the trajectory point on the rolling wheel by adopting a CET and a PET [18]. Therefore, a CET and a PET were selected for the magnet shape in an SPMSM.

The trajectory equation for the epicycloid curve, which forms the basis of the CET and PET, is described. An epicycloid curve is a trajectory drawn by a point on the circumference of a wheel with radius R_{fc} rolling on a fixed circle of radius R_{fc} . The trajectory is indicated by the purple line in Fig. 1.

Fig. 2 shows an enlarged view of a part of the epicycloid curve shown in Fig. 1. In Fig. 2, P_{ec} represents the point on the epicycloid curve and is given in the vector loop form of Equation (1).

$$\overrightarrow{O_{fc}P_{ec}} = \overrightarrow{O_{fc}O_{rc}} + \overrightarrow{O_{rc}P_{ec}} \quad (1)$$

TABLE 1. Cycloid curve type.

Location of the point	Circle rolls outside a fixed circle	Circle rolls inside a fixed circle
	Epicycloid	Hypocycloid
On the circumference		
	CET: Curtate Epitrochoid	Curtate Hypotrochoid
Inside the circumference		
	PET: Prolate Epitrochoid	Prolate Hypotrochoid
Outside the circumference		

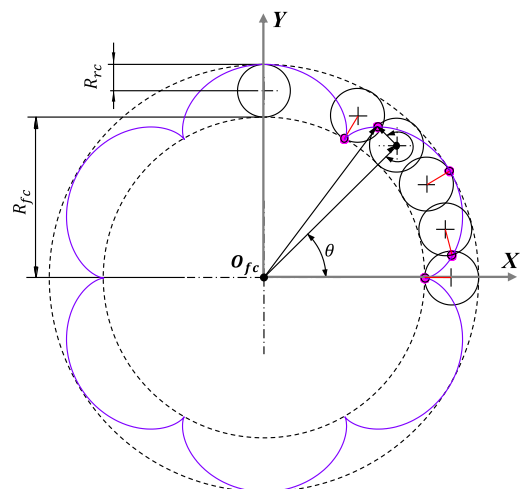


FIGURE 1. Epicycloid curve.

When the vector $\overrightarrow{O_{fc}P_{ec}}$ is at an angle θ with respect to the X axis, the angle between the vectors $\overrightarrow{O_{fc}O_{rc}}$ and $\overrightarrow{O_{rc}P_{ec}}$ is $n\theta$,

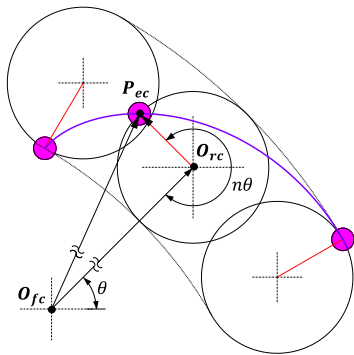


FIGURE 2. Enlargement of the epicycloid curve.

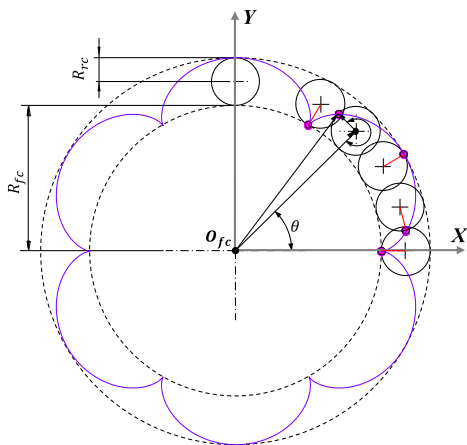


FIGURE 3. CET curve.

where n indicates the wavenumbers for an epicycloid and can be expressed as follows:

$$n = \frac{R_{fc}}{R_{rc}}. \quad (2)$$

When P_{ec} is presented in a polar coordinate system using Equation (1), it becomes

$$P_{et} = (R_{fc} + R_{rc}) e^{j\theta} - R_{rc} e^{j(n+1)\theta}. \quad (3)$$

The Cartesian coordinate values of P_{ec} can be expressed as follows:

$$\begin{cases} x_{et} = (R_{fc} + R_{rc}) \cos \theta - (R_{fc} + R_{rc}) \cos ((n + 1) \theta) \\ y_{et} = (R_{fc} + R_{rc}) \sin \theta - (R_{fc} + R_{rc}) \sin ((n + 1) \theta). \end{cases} \quad (4)$$

In the case of a CET, the trajectory point of the CET exists inside the rolling circle, as shown in Fig. 3.

The eccentricity ϵ_{cet} of the CET satisfies

$$\epsilon_{cet} < R_{rc}. \quad (5)$$

The Cartesian coordinate values of P_{cet} for a CET curve are calculated in the same manner as in Equations (1)–(4) and can be expressed as follows:

$$\begin{cases} x_{cet} = (R_{fc} + R_{rc}) \cos \theta - \epsilon_{cet} \cos ((n + 1) \theta) \\ y_{cet} = (R_{fc} + R_{rc}) \sin \theta - \epsilon_{cet} \sin ((n + 1) \theta). \end{cases} \quad (6)$$

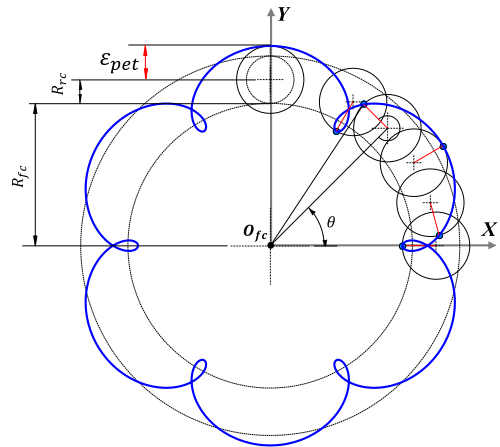


FIGURE 4. PET curve.

TABLE 2. Specifications of EPS motor.

Type	SPMSM
Phase/pole/slot	3/6/9
Stator diameter	84 mm
Rotor diameter	38 mm
Magnet thickness	3 mm
Maximum torque	5 Nm

In the case of a PET curve, the curve exists outside the rolling circle, as shown in Fig. 4.

The eccentricity ϵ_{cet} of the PET satisfies

$$\epsilon_{pet} > R_{rc}. \quad (7)$$

The Cartesian coordinate values of P_{pet} for a PET curve are calculated in the same way as those for a CET curve and can be expressed as follows:

$$\begin{cases} x_{pet} = (R_{fc} + R_{rc}) \cos \theta - \epsilon_{pet} \cos (\theta \cdot (n + 1)) \\ y_{pet} = (R_{fc} + R_{rc}) \sin \theta - \epsilon_{pet} \sin (\theta \cdot (n + 1)). \end{cases} \quad (8)$$

III. MAGNET DESIGN USING CYCLOID CURVE

A. ANALYSIS MODEL

In this study, the proposed method for magnet design was applied to an EPS system. Table 2 presents the specifications.

B. DEFINITION OF δq

In this study, an evaluation index δq is used to compare the performances for the conventional and proposed curves [7]. Here, δq represents the air-gap length on the q-axis, which has an electrical phase difference of 90° with the d-axis (i.e., the center axis of the rotor magnet flux). The value of δq is described in Fig. 7. In this paper, δq is defined as the distance from the intersection point of the extended curve for the magnet shape (red dotted arc in Fig. 5) and the q axis to the intersection point of the rotor outer radius R_{mo} and the q axis. In Fig. 7, τ_p , τ_a , and R_{ri} represent the pole pitch, pole arc, and rotor core diameter, respectively.

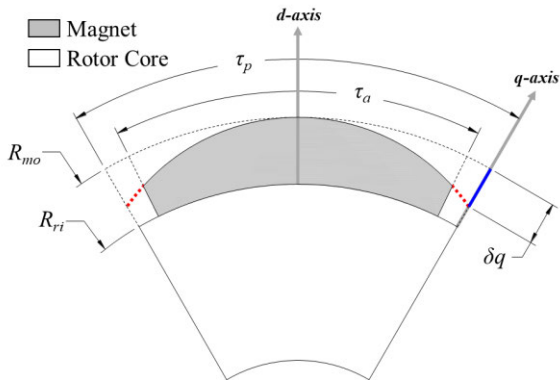


FIGURE 5. Definition of δq .

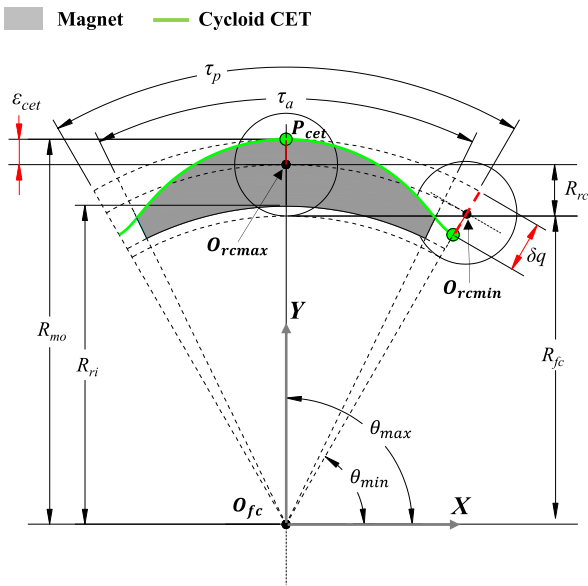


FIGURE 6. Magnet shape design using the CET curve.

C. CET CURVE

The magnet design of a CET curve is described in Fig. 6. In Fig. 6, the number of poles N_p is equal to n , as indicated by Equation (2).

The minimum length from the origin to the point on the CET curve occurs at the angle θ_{min} between the line $\vec{O_{fc}O_{rcmin}}$ and the X axis. For the CET curve, when considering the eccentricity ϵ_{cet} , θ_{min} can be expressed as follows:

$$\theta_{min} = n \frac{2\pi}{N_p}, \tag{9}$$

where n ranges from 0 to $N_p - 1$. When θ_{min} is substituted into Equation (6), the minimum length L_{cetmin} is calculated as follows:

$$L_{cetmin} = R_{fc} + R_{rc} - \epsilon_{cet}. \tag{10}$$

The maximum length L_{cetmax} from the origin O_{fc} to a point along the CET curve occurs at the angle θ_{max} . Here, L_{cetmax} is calculated using the following equation:

$$\theta_{max} = \frac{\pi(2n+1)}{N_p}. \tag{11}$$

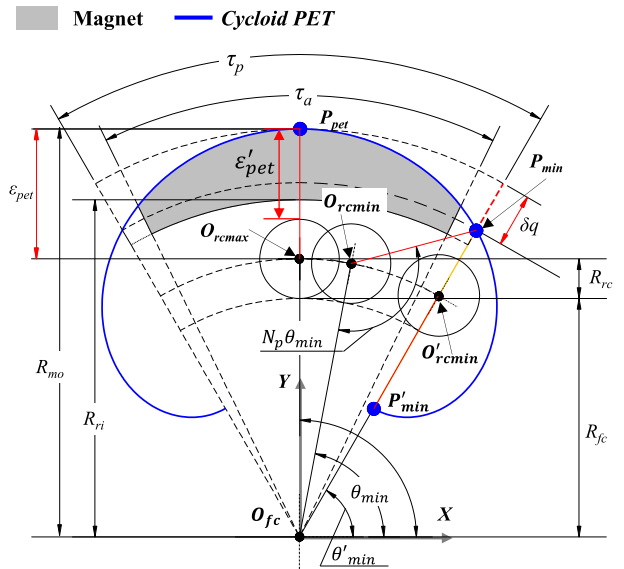


FIGURE 7. Magnet shape design using PET curve.

The maximum length L_{cetmax} is equal to the known parameter R_{mo} , as shown in Fig. 5, which is calculated using Equation (12) when θ_{max} is substituted into Equation (6).

$$R_{mo} = L_{cetmax} = R_{fc} + R_{rc} + \epsilon_{cet}. \tag{12}$$

The length δq is equal to the distance between L_{cetmin} and L_{cetmax} , as shown in Fig. 5. Here, δq can be expressed as follows:

$$\delta q = 2\epsilon_{cet}. \tag{13}$$

To define the magnet shape using the CET curve for δq , the unknown parameters R_{fc} and R_{rc} can be expressed as follows:

$$R_{rc} = \frac{2R_{mo} - \delta q}{2(N_p + 1)}. \tag{14}$$

$$R_{fc} = N_p R_{rc}. \tag{15}$$

D. PET CURVE

A magnet shape design with a PET curve is described in Fig. 7. Because the eccentricity ϵ_{pet} of the PET curve is higher than that of the CET curve, it is calculated as follows:

$$\epsilon_{pet} = R_{rc} + \epsilon'_{pet}. \tag{16}$$

Using Equations (8) and (15), the Cartesian coordinates of the PET curve can be expressed as follows:

$$\begin{cases} x_{pet} = (R_{fc} + R_{rc}) \cos \theta - (R_{rc} + \epsilon'_{pet}) \cos((N_p + 1)\theta) \\ y_{pet} = (R_{fc} + R_{rc}) \sin \theta - (R_{rc} + \epsilon'_{pet}) \sin((N_p + 1)\theta). \end{cases} \tag{17}$$

Similar to the case of a CET curve, the maximum distance L_{petmax} from the origin O_{fc} to the PET curve can be expressed as follows:

$$R_{mo} = L_{petmax} = R_{fc} + 2R_{rc} + \epsilon'_{pet}. \tag{18}$$

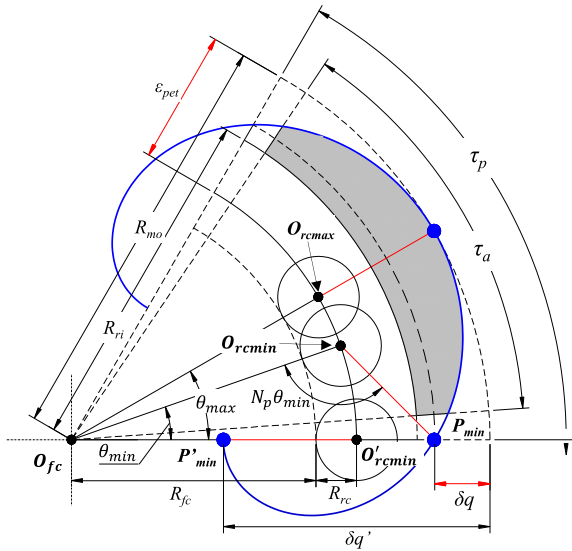


FIGURE 8. δq calculation for PET curve.

For a PET curve, the unknown parameters R_{fc} and R_{rc} can be obtained using Equation (16). Here, R_{rc} is identical to that in Equation (14) and can be expressed as follows:

$$R_{rc} = \frac{R_{mo} - \varepsilon'_{pet}}{N_p + 2}, \quad (19)$$

where ε'_{pet} is the unknown parameter in Equation (18). However, R_{fc} must be expressed in terms of δq to define the PET curve. In the case of the PET curve, ε'_{pet} is higher than that of the CET curve. Therefore, the starting point begins with point P'_{min} inside R_{fc} . To define δq of the PET curve, it is necessary to calculate the coordinate values of point P_{min} , as shown in Fig. 7.

Here, P_{min} is the endpoint of line $\overrightarrow{O_{rc}P_{min}}$ when R_{rc} is rotated by the angle $N_p\theta_{min}$. For an easier calculation, if P_{min} is on the X axis, as shown in Fig. 8, it is possible to satisfy Equation (16). When $y_{pet} = 0$, as in Equation (16), this equation can be transformed into a higher-order equation to determine the value of θ_{min} .

Because this equation becomes an $N_p + 1$ -order equation, δq is calculated using the iteration method, as shown in Fig. 9. The iteration method in Fig. 8 calculates δq by applying $R_{mo} = 19$ and $N_p = 6$, as shown in Table 2.

E. ECCENTRIC CIRCLE

In general, to reduce the cogging torque, an eccentric curve is employed [11]–[13]. In this study, an eccentric curve is used for comparison with the cycloid curve. To apply an eccentric circle to a magnet shape, the eccentricity ε_{ec} and circle radius R_{ec} should be calculated using the known parameters δq , R_{mo} , and N_p described above. The known and unknown parameters for the eccentric curve are described in Fig. 10. The circular equation for R_{mo} can be expressed as follows:

$$x^2 + y^2 = R_{mo}^2. \quad (20)$$

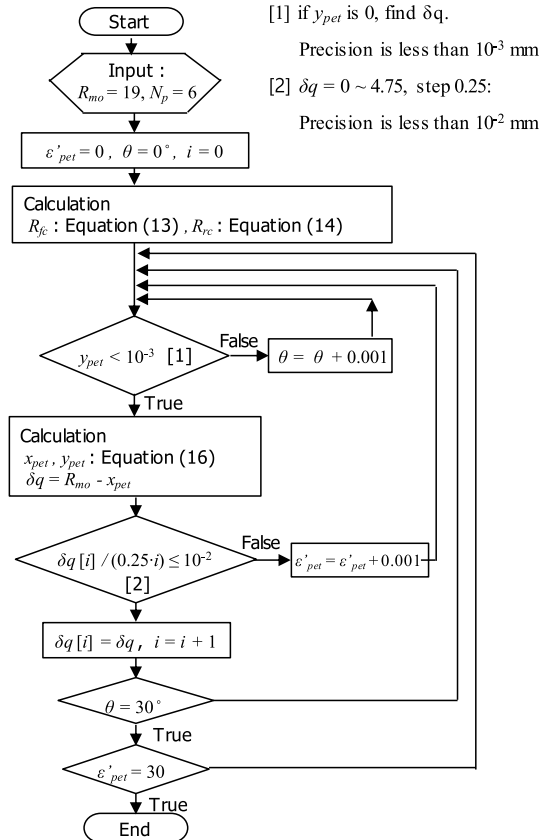


FIGURE 9. Flow chart of δq calculation for the PET curve.

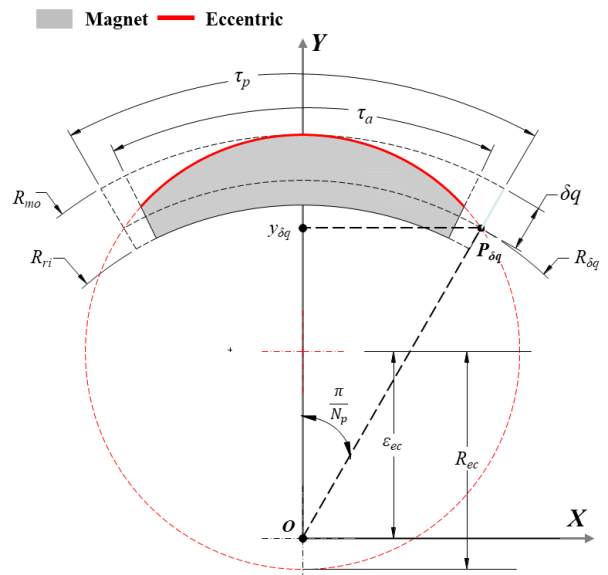


FIGURE 10. Magnet shape design with an eccentric curve.

The circular equation passing point $P_{\delta q}$ with radius $R_{\delta q}$ can be expressed as follows:

$$x^2 + y^2 = R_{\delta q}^2 = (R_{mo} - \delta q)^2. \quad (21)$$

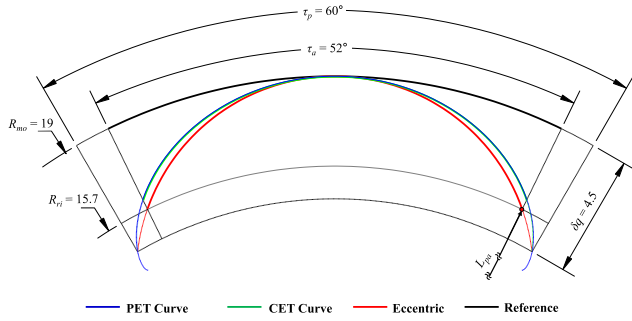


FIGURE 11. Magnet shape at $\delta q = 4.5$.

The circular equation of an eccentric curve applied to the magnet shape can be expressed as follows:

$$x^2 + (y - \varepsilon_{ec})^2 = R_{ec}^2 = (R_{mo} - \varepsilon_{ec})^2. \quad (22)$$

The Y axis value $y_{\delta q}$ of the intersection point between Equations (20) and (21) can be expressed as follows:

$$y_{\delta q} = (R_{mo} - \delta q) \cos\left(\frac{\pi}{N_p}\right). \quad (23)$$

Equation (29) for x^2 can be expressed as follows:

$$x^2 = (R_{mo} - \delta q)^2 - y^2. \quad (24)$$

The unknown parameter ε_{ec} can be calculated by substituting Equations (22) and (23) into (21).

$$\varepsilon_{ec} = \frac{\delta q^2 - 2R_{mo}\delta q}{2(y_{\delta q} - R_{mo})}. \quad (25)$$

The unknown parameter R_{ec} is calculated using the geometric relationship shown in Fig. 10.

$$R_{ec} = R_{mo} - \varepsilon_{ec}. \quad (26)$$

IV. MAGNET SHAPE ANALYSIS

The motor performances are analyzed using the finite-element method (FEM) for the magnet shape designs of cycloid and eccentric curves. To analyze the performance of the motor, no-load and load analyses are conducted. For the no-load analysis, the back EMF and cogging torque are analyzed, whereas for the load analysis, the average torque and torque ripple are analyzed.

A. MAGNET SHAPE DESIGN MODEL

Fig. 11 shows the magnet shape for comparing the cycloid and eccentric curves at the specific value of $\delta q = 4.5$. The solid lines represent the magnet shapes for τ_a . The dotted lines represent the trajectory curve for τ_p . In Fig. 11, L_{pa} indicates the length from the origin to the intersection point of each curve for τ_p . The value of L_{pa} exhibits little difference between the PET and CET at $\delta q = 4.5$, as indicated by Table 3. As shown in Table 3, the reference curve has a value of $\delta q = 0$, and its objective is to compare the performances of the cycloid and eccentric curve models.

TABLE 3. Comparison of L_{pa} .

Curve Model	PET	CET	Eccentric	Reference
δq [mm]	4.5	4.5	4.5	0
L_{pa} [mm]	16.10	16.08	15.71	19

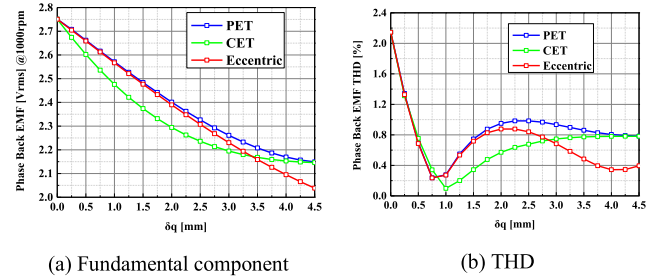


FIGURE 12. Fundamental component and THD for the back EMF.

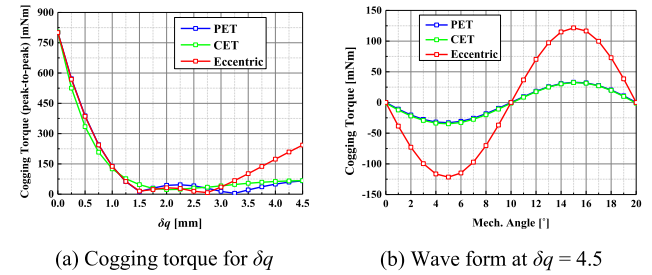


FIGURE 13. Cogging torque and waveform.

B. NO-LOAD ANALYSIS

A no-load analysis was conducted to verify the electrical characteristics, such as the back EMF and cogging torque with no input currents.

Fig. 12 shows the fundamental component and total harmonic distortion (THD) of the back EMF for each curve according to δq . The fundamental component and THD of the back EMF for a PET and CET cycloid converge at constant values. However, the eccentric curve decreases sharply. Therefore, the changes in the fundamental component and THD for a cycloid curve are stable compared with those for an eccentric curve.

Fig. 13(a) shows the cogging torque (peak-to-peak value) for δq . In the case of cycloid curves, the fundamental component converges to a constant value, in contrast to the eccentric curve. To compare the cycloid and eccentric curves, Fig. 13(b) shows the one-period waveform of the cogging torque at a specific value of $\delta q = 4.5$. In general, the one-period angle of the cogging torque θ_{1ct} , which is the mechanical angle, can be expressed as follows [19]:

$$\theta_{1ct} = \frac{360}{LCM(N_s, N_p)}. \quad (27)$$

In Equation (26), LCM and N_s indicate the least common multiplier and the number of slots, respectively. In this study, $\theta_{1ct} = 20^\circ$, according to Equation (26).

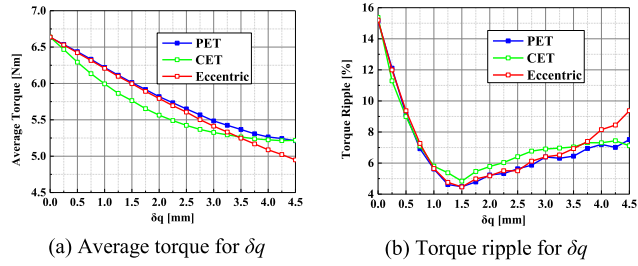


FIGURE 14. Average torque and torque ripple at the maximum torque.

TABLE 4. Magnets and rotor assemblies.

Prototype	Cycloid	Eccentric	Reference
Magnet			
Rotor Assembly			

C. LOAD ANALYSIS

First, the demagnetization of all magnets, including the lower thickness on both sides of each magnet, was verified in the cycloid and eccentricity models via FEA.

The average torque and torque ripple were analyzed through a load analysis for δq by supplying the current corresponding to the maximum torque, as shown in Table 2.

Fig. 14(a) shows the average torque for δq . For a cycloid, the change in the average torque is similar to that of the fundamental component for a back EMF, as shown Fig. 12(a). This confirms that the back EMF is proportional to the torque [19]. Fig. 14(b) shows the torque ripple for δq . For a cycloid, the value decreases and converges to a constant. For an eccentric curve, the value decreases and increases sharply. The change in the torque ripple is similar to that of the cogging torque, as shown in Fig. 13(a)

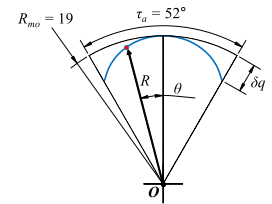
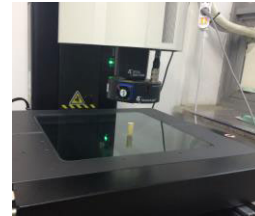
V. EXPERIMENT

A. PROTOTYPE

To verify the performances of the cycloid and eccentric curves, the manufacturing tolerance should be considered. The delta q index was adopted by considering two factors: the fulfillment of the target performance and robust design considering the tolerance on dimensions. To compare the performances of the cycloid and eccentric curves according to the foregoing considerations, a value of 4.5 was selected for δq , as shown in Fig. 11. In the case of $\delta q = 4.5$, the PET and CET models can be regarded as a single model, because there are no differences between the two models with regard to the geometric and motor characteristics, as discussed in Chapter III. Therefore, the PET and CET models with

TABLE 5. Measured shape of magnet.

PET	Eccentric	Reference



(a) Equipment

(b) Curve (blue line)

FIGURE 15. Equipment and curve for the measurement.

TABLE 6. Measurement errors for magnet surface.

	Prototype	PET	Eccentric	Reference
Measurement	Maximum	0.07	0.06	0.04
Errors [mm]	Minimum	-0.04	0.02	-0.01

$\delta q = 4.5$ are referred to as the cycloid models. Table 4 presents the magnets manufactured for the cycloid, eccentric, and reference models selected from Table 3, as well as their prototypes assembled into the rotor core.

Table 5 presents the measurement results of the magnet shapes for the PET, eccentric, and reference models assembled in the rotor (from Table 4). For the measurement, noncontact three-dimensional scanning equipment was used, as shown in Fig. 15(a). The number of measured data for each curve was 720, as indicated by the blue lines in Fig. 15(b).

In Table 5, the red dots represent the measured data, and the black line represents the designed shape for a one-pole magnet.

Table 6 shows the measured errors of the magnet shape for the cycloid, eccentric, and reference models. The measured errors indicate the difference between the measured and designed magnet shape distances (blue line) for the radial direction distance R , as shown in Fig. 15(b).

B. NO-LOAD TEST: COGGING TORQUE

The cogging torque was measured for each prototype, as shown in Table 7. The measurement speed was 1 rpm.

The cogging-torque waveforms for the prototype from the FEA and measurement results are shown in Fig. 16.

Table 8 presents the cogging torque (peak-to-peak) for the FEA and test results. For the PET and eccentric model, the cogging-torque measurements were higher than the FEA results.

The difference in the cogging torque is attributed to a manufacturing error. As shown in Table 8, the manufacturing error was smaller for the cogging torque of the PET than for that of the eccentric model, as there was little difference in

TABLE 7. Cogging torque test setup.

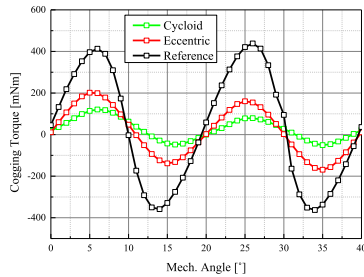
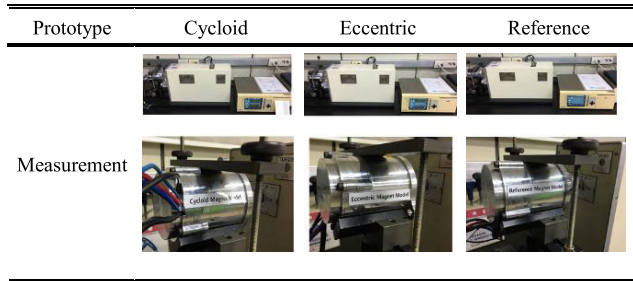


FIGURE 16. Test results for cogging torque waveform.

TABLE 8. FEA and test results for the cogging torque.

Prototype	Cycloid	Eccentric	Reference
Test [mNm]	182	375	805
FEA [mNm]	67	243	800

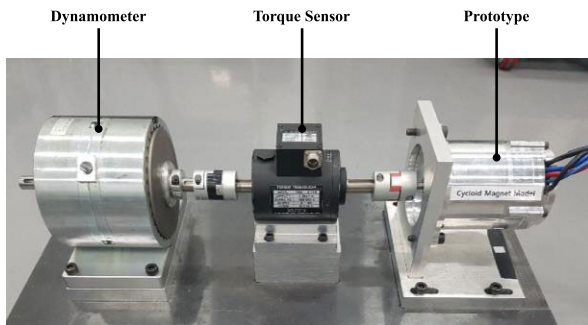


FIGURE 17. Load-test setup.

the cogging torque between the test and FEA results for the PET.

For the reference model, the measured values were similar to the FEA results.

C. LOAD TEST: AVERAGE TORQUE AND TORQUE RIPPLE

A current is supplied at the maximum torque to verify the average torque and torque ripple. The $I_d = 0$ control method was applied using an SPMSM [19]. Fig. 17 shows the test equipment used for the torque measurement.

Table 9 shows that the errors in the test results of the FEM were $\leq 1.2\%$ for the average torque. Additionally, it was confirmed that the average torque of the PET model was improved compared with that of the eccentric model. In the case of the torque ripple, the errors of the test results com-

TABLE 9. Torque measurements of FEA and test results.

	Prototype	Cycloid	Eccentric	Reference
Average Torque [Nm]	FEA	5.36	4.99	6.73
	Test	5.15	5.08	6.72
Torque Ripple [%]	FEA	4.9	6.4	12.6
	Test	6.37	9.2	11.96

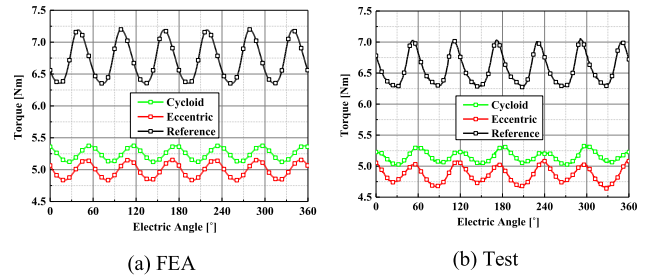


FIGURE 18. Torque waveform for FEA and test results.

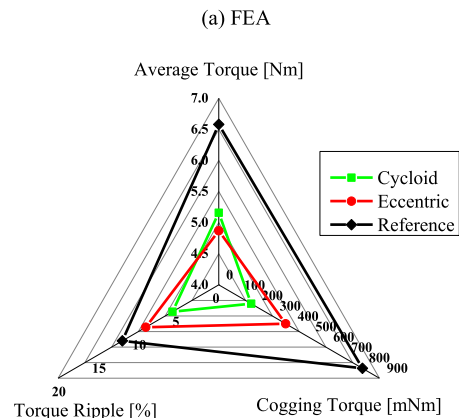
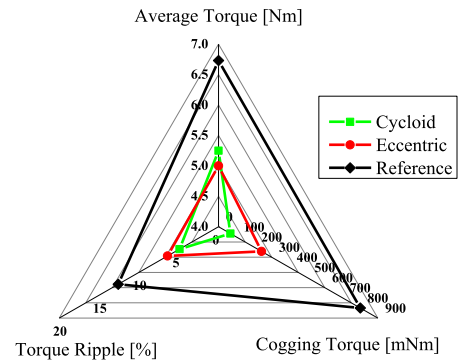


FIGURE 19. FEA and test results for prototypes.

pared with the FEA results were large, whereas the FEA results exhibited the same tendency as the measured values when a prototype was used. Even in this case, the torque ripple of the PET model was reduced compared with that of the eccentric model. Fig. 18 shows the FEA and test results for the torque waveform with an electrical angle of 360°.

Fig. 19 shows the FEA and test results of prototypes for the cogging torque, average torque, and torque ripple. The

TABLE 10. Comparison of normalized value based on reference.

	Prototype	Cycloid	Eccentric	Reference (Base)
FEA	Average Torque	0.80	0.74	
	Cogging Torque	0.08	0.30	1
	Torque Ripple	0.39	0.51	
Test	Average Torque	0.77	0.76	
	Cogging Torque	0.23	0.47	1
	Torque Ripple	0.53	0.77	

performances of the PET model were improved compared with those of the eccentric model.

VI. CONCLUSION

The cogging torque and torque ripple are the key qualities of a motor for enhancing the control precision and driving sensibility of vehicles, robots, and other devices. Thus, it is necessary to reduce the cogging torque and torque ripple. In this study, a design method for the magnet shape using a cycloid curve was developed. According to the reference design results, a PET and a CET were selected among the different cycloid-curve types.

To compare the proposed curves with the conventional curves applied to the magnet shape, the evaluation index δq was employed. Using δq , a design method was developed for the cycloid (PET and CET) and conventional curves. Prototypes were manufactured to verify FEA results. For a comparison and evaluation of the prototypes using the proposed cycloid and conventional curves, $\delta q = 4.5$ was applied.

The results of the FEA and experiment indicated that the motor characteristics for a cycloid-curve magnet shape were improved compared with those for a conventional curved magnet. Therefore, using the proposed cycloid curve, a cogging torque and torque ripple can be applied without reducing the average torque.

REFERENCES

- [1] J. Jang, S.-G. Cho, S.-J. Lee, K.-S. Kim, J.-M. Kim, J.-P. Hong, and T. H. Lee, "Reliability-based robust design optimization with kernel density estimation for electric power steering motor considering manufacturing uncertainties," *IEEE Trans. Magn.*, vol. 51, no. 3, Mar. 2015, Art. no. 8001904.
- [2] C. F. Wang, J. X. Shen, P. C. K. Luk, W. Z. Fei, and M. J. Jin, "Design issues of an IPM motor for EPS," *COMPEL Int. J. Comput. Math. Elect. Electron. Eng.*, vol. 31, no. 1, pp. 71–87, 2011.
- [3] X. Sun, K. Diao, G. Lei, Y. Guo, and J. Zhu, "Study on segmented-rotor switched reluctance motors with different rotor pole numbers for BSG system of hybrid electric vehicles," *IEEE Trans. Veh. Technol.*, vol. 68, no. 6, pp. 5537–5547, Jun. 2019.
- [4] X. Sun, B. Su, S. Wang, Z. Yang, G. Lei, J. Zhu, and Y. Guo, "Performance analysis of suspension force and torque in an IBPMSM with V-shaped PMs for flywheel batteries," *IEEE Trans. Magn.*, vol. 54, no. 11, Nov. 2018, Art. no. 8105504.
- [5] Z. Shi, X. Sun, Y. Cai, Z. Yang, G. Lei, Y. Guo, and J. Zhu, "Torque analysis and dynamic performance improvement of a PMSM for EVs by skew angle optimization," *IEEE Trans. Appl. Supercond.*, vol. 29, no. 2, Mar. 2019, Art. no. 0600305.
- [6] Y.-K. Kim, J.-J. Lee, J.-P. Hong, and Y. Hur, "Analysis of cogging torque considering tolerance of axial displacement on BLDC motor by using a stochastic simulation coupled with 3-D EMCN," *IEEE Trans. Magn.*, vol. 40, no. 2, pp. 1244–1247, Mar. 2004.
- [7] A. Yoneda, T. Miyoshi, and Y. Shimizu, "Cogging torque target and design of motor for EPS," in *Proc. SAE World Congr. Exhib.*, Detroit, MI, USA, Apr. 2006.
- [8] Z. Q. Zhu, Z. Azar, and G. Ombach, "Influence of additional air gaps between stator segments on cogging torque of permanent-magnet machines having modular stators," *IEEE Trans. Magn.*, vol. 48, no. 6, pp. 2049–2055, Jun. 2012.
- [9] P. Lazari, J. Wang, and B. Sen, "3-D effects of rotor step-skews in permanent magnet-assisted synchronous reluctance machines," *IEEE Trans. Magn.*, vol. 51, no. 11, Nov. 2015, Art. no. 8112704.
- [10] S. A. Evans, "Salient pole shoe shapes of interior permanent magnet synchronous machines," in *Proc. 19th Int. Conf. Elect. Mach. (ICEM)*, Rome, Italy, Sep. 2010, pp. 1–6.
- [11] R. Islam, I. Husain, A. Fardoun, and K. McLaughlin, "Permanent-magnet synchronous motor magnet designs with skewing for torque ripple and cogging torque reduction," *IEEE Trans. Ind. Appl.*, vol. 45, no. 1, pp. 152–160, Jan. 2009.
- [12] J. Hur and B. W. Kim, "Rotor shape design of an interior PM type BLDC motor for improving mechanical vibration and EMI characteristics," *J. Elect. Eng. Technol.*, vol. 5, no. 3, pp. 462–467, Sep. 2010.
- [13] M. A. Khan, I. Husain, M. R. Islam, and J. T. Klass, "Design of experiments to address manufacturing tolerances and process variations influencing cogging torque and back EMF in the mass production of the permanent-magnet synchronous motors," *IEEE Trans. Ind. Appl.*, vol. 50, no. 1, pp. 346–355, Jan./Feb. 2013.
- [14] F. T. Jorgensen, T. O. Andersen, and P. O. Rasmussen, "The cycloid permanent magnetic gear," *IEEE Trans. Ind. Appl.*, vol. 44, no. 6, pp. 1659–1664, Nov./Dec. 2008.
- [15] C.-U. Ricardo, "Cycloidal magnetic gear speed reducer," *Mod. Mech. Eng.*, vol. 3, no. 4, pp. 147–151, Nov. 2013.
- [16] K. Davey, L. McDonald, and T. Hutson, "Axial flux cycloidal magnetic gears," *IEEE Trans. Magn.*, vol. 50, no. 4, Apr. 2014, Art. no. 8100607.
- [17] M. Jamadar and A. Jose, "Development of in-house competency to build compact gerotor oil pump for high speed diesel engine application," SAE Tech. Paper 2013-01-2738, 2013.
- [18] W. S. Jonathon, "Unified approach to cycloid drive profile, stress, and efficiency optimization," *J. Mech. Des.*, vol. 132, no. 2, Feb. 2010, Art. no. 024503.
- [19] M. S. Lim, S. H. Chai, J. S. Yang, and J. P. Hong, "Design and verification of 150 krpm PMSM based on experiment results of prototype," *IEEE Trans. Ind. Electron.*, vol. 62, no. 12, pp. 7827–7836, Dec. 2015.
- [20] Y. Zhou, H. Li, G. Meng, S. Zhou, and Q. Cao, "Analytical calculation of magnetic field and cogging torque in surface-mounted permanent-magnet machines accounting for any eccentric rotor shape," *IEEE Trans. Ind. Electron.*, vol. 62, no. 6, pp. 3438–3447, Jun. 2015.
- [21] Y. Cho, K.-B. Lee, J.-H. Song, and Y. I. Lee, "Torque-ripple minimization and fast dynamic scheme for torque predictive control of permanent-magnet synchronous motors," *IEEE Trans. Power Electron.*, vol. 30, no. 4, pp. 2182–2190, Apr. 2015.
- [22] W. Q. Chu and Z. Q. Zhu, "Investigation of torque ripples in permanent magnet synchronous machines with skewing," *IEEE Trans. Magn.*, vol. 49, no. 3, pp. 1211–1220, Mar. 2013.
- [23] S.-I. Kim, J.-Y. Lee, Y.-K. Kim, J.-P. Hong, Y. Hur, and Y.-H. Jung, "Optimization for reduction of torque ripple in interior permanent magnet motor by using the Taguchi method," *IEEE Trans. Magn.*, vol. 41, no. 5, pp. 1796–1799, May 2005.
- [24] T. J. E. Miller and J. R. Hendershot, *Design of Brushless Permanent-Magnet Machines*. Oxford, U.K.: Oxford Univ. Press, 2010.



HYEON-JIN PARK received the B.S. degree in mechanical engineering from Hanyang University, Seoul, South Korea, in 2011. He is currently pursuing the integrated M.S. and Ph.D. degrees in automotive engineering with Hanyang University, Seoul. From 2014 to 2017, he was a Research Engineer in Keayang, South Korea. His research interests include electromagnetic field analysis and electric machine design.



MYUNG-SEOP LIM received the bachelor's degree in mechanical engineering and the master's and Ph.D. degrees in automotive engineering from Hanyang University, Seoul, South Korea, in 2012, 2014, and 2017, respectively.

From 2017 to 2018, he was a Research Engineer with Hyundai Mobis, Yongin, South Korea. From 2018 to 2019, he was an Assistant Professor with Yeungnam University, South Korea. Since 2019, he has been with Hanyang University, where he is currently an Assistant Professor. His research interests include electromagnetic field analysis and electric machinery for mechatronics systems, such as automotive and robot applications.



CHUNG-SEONG LEE received the B.S. degree in automation engineering from Inha University, Incheon, South Korea, in 2000, the M.S. degree in machine intelligence engineering from Tohoku University, Sendai, Japan, in 2002, and the Ph.D. degree in automotive engineering from Hanyang University, Seoul, South Korea, in 2017. He is currently a Researcher with Mando Corporation, South Korea. His research interests include electromagnetic field analysis and electric machine design.

• • •